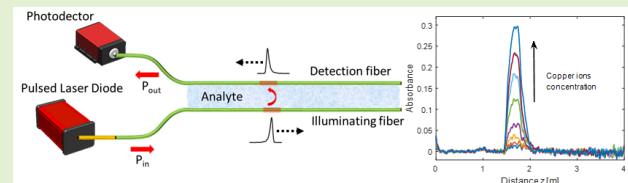


Light Diffusing Optical Fiber Sensor for Distributed Optical Absorption Spectroscopy and Chemical Sensing

Gianluca Persichetti¹, Genni Testa¹, Pasquale Imperatore¹, *Member, IEEE*,
and Romeo Bernini¹, *Member, IEEE*

Abstract—An optical fiber sensor system for distributed optical absorption spectroscopy based on light diffusing optical fiber is proposed and evaluated. The sensor is composed by two light-diffusing glass fibers radiatively coupled. The light from a pulsed laser diode (PLD) propagates along the first fiber and is locally diffused out into the medium between the fibers. The light transmitted by the medium is partially collected by the second fiber and detected at the end of the fiber by an optical time-domain reflectometry (OTDR) detection scheme. The system permits distributed measurements of the optical absorption properties of the sample medium between the fibers. The experimental results confirm the possibility of distributed measurements with a spatial resolution of about 17 cm over 4 m of measurement range. Distributed chemical sensing has also been evaluated by measuring the absorption of water solutions containing copper ions. A limit of detection (LOD) of 710 ppm has been achieved.

Index Terms—Distributed sensors, fiber-optic sensors, light diffusing fiber (LDF), optical spectroscopy.



I. INTRODUCTION

OPTICAL fiber sensors are a powerful tool in a lot of application fields. They offer several advantages, including small weight, low size, immunity to electromagnetic interference, and possibility of remote operation. In particular, in last years, there was a great interest in their application in the chemical and biochemical sensing.

Single point sensor based on surface plasmon resonance (SPR) [1], [2], [3], [4], [5], [6] and localized SPR (LSPR) [7], [8] has been proposed. These approaches might be adequate for many applications. However, when many measurement points are required, the distributed sensing capabilities are an advantage.

Distributed fiber optic sensors enable high-resolution continuous measurements over long distance [9], [10]. Currently,

Manuscript received 31 October 2022; revised 7 December 2022; accepted 7 December 2022. Date of publication 19 December 2022; date of current version 31 January 2023. This work was supported in part by the Italian Ministry of Research and Education through the Frame of Project of National Operational Programme (PON) Autonomous Robotics for the Extended Ship (ARES) under Grant ARS01_00682. The associate editor coordinating the review of this article and approving it for publication was Prof. Santosh Kumar. (*Corresponding author: Romeo Bernini.*)

The authors are with the Institute for Electromagnetic Sensing of the Environment (IREA), National Research Council of Italy (CNR), 80124 Naples, Italy (e-mail: persichetti.g@irea.cnr.it; testa.g@irea.cnr.it; imperatore.p@irea.cnr.it; bernini.r@irea.cnr.it).

Digital Object Identifier 10.1109/JSEN.2022.3229133

This work is licensed under a Creative Commons Attribution 4.0 License. For more information, see <https://creativecommons.org/licenses/by/4.0/>

these sensors employ low-loss single/multimode glass or polymeric fiber as sensing element [11], [12], [13], [14]. They are mainly based on optical phenomena, such as Rayleigh, Brillouin, or Raman scattering that are intrinsically present in optical fibers [15], [16], [17], [18]. The spatial information is usually resolved by optical time-domain reflectometry (OTDR), launching an optical pulse into the fiber and measuring the variation of the backscattered light measured as a function of time [19]. The spatial location can be calculated by taking into account the time-of-flight inside the fiber. A lot of approaches have been developed in order to detect physical external perturbations along the sensing fiber, such as temperature, strain, pressure, and so on, by measuring the variations in amplitude, frequency, polarization, or phase of the backscattered sensing light [10], [20], [21]. Over the past decades, there was a great effort to extend distributed fiber sensing from the physical to chemical domain [22], [23]. However, this objective is intrinsically challenging because, typically, common optical fibers are chemically inert and an additional sensing element is required to convert the chemical information into a signal measurable by the optical fiber, such as strain/temperature [15], optical loss [24], or optical absorption [25].

Most of the distributed chemical sensing methods are based on the interaction of the evanescent field of the fiber core modes with suitable sensing layers that act as fiber

cladding. Both fluorescence-based and absorption-modulated processes have been investigated [25], [26]. Typically, in these approaches, a chemical dye is immobilized into a suitable fiber cladding material. The interaction of the dye with the chemical substance alters the optical characteristics of the fiber, via the evanescent fields, and induces a change in the absorption/fluorescence backscatter signal.

Using these approaches, a number of distributed chemical optical fiber sensors have been proposed for sensing pH [27], [28] and oxygen concentration [29]. However, one of the main difficulty of these approaches is related to the development and the deposition on the fiber of a suitable sensing layer materials that meet the required chemical and optical properties.

Photonic bandgap hollow-core fibers have generated a particular interest for chemical sensing because of the possibility of guiding light inside the hollow core enables a large light–material interaction [30]. However, while these fibers have been fruitfully employed for single point sensing, their application in distributed sensing has been strongly limited because the analyte can enter only at the open end faces of the fiber. In order to overcome this problem, manufacturing approaches like drilling holes on the outer cladding [30] or by opening slots on the side have been proposed.

Optical absorption spectroscopy represents a common approach to water and gas monitoring as it offers the potential of label-free spectral detection and identification of specific analytes in a very easy way [31], [32].

In this article, for the first time, a distributed fiber optic sensor for the continuous spatial measurement of the optical absorption of the medium between the fibers is proposed.

The sensor consists of two parallel light diffusing fibers (LDFs) that are radiatively coupled. LDF is an optical fiber that radially diffuses the light outward from the core due to the presence of nanometric scattering centers in the core [33]. By controlling the fabrication process, it is possible to obtain a uniform scattering of the light that propagates through the fiber circumference and along the length of the optical fiber. This fiber has been intended for illumination purposes, but sensing applications have also been recently demonstrated [34], [35].

In the proposed sensor, the illuminating fiber is connected to a pulsed laser diode (PLD). The narrow light pulse propagates along the fiber and locally diffuses outside the core. A portion of this scattered light, after propagating through the sample medium between the fibers, is coupled into the second fiber and is finally delivered to an OTDR photodetection system. By converting the time information into the spatial one, it is possible to perform distributed measurements of the optical absorption properties of the medium between the fibers.

Differently from the convectional evanescent field techniques, this approach allows the coupling between the light and the sample at very large distances compared to the working wavelengths, thus increasing the path length that light travels through the sample and enhancing the absorption sensitivity. Furthermore, the power coupling occurs over a very broadband wavelength range of more than 1000 nm [36]. Finally, it is worth emphasizing that the proposed configuration does not require any manipulation of the optical fiber, such as cladding

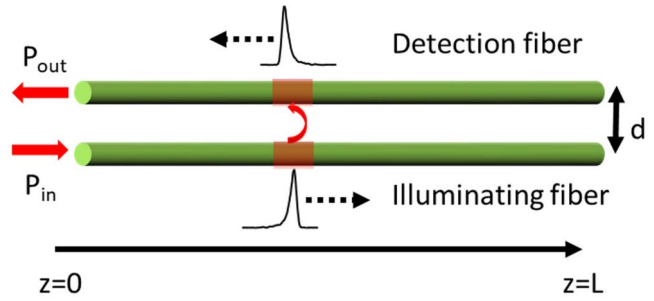


Fig. 1. Sensing principle layout.

removal, etching, and bending, in this way greatly simplifying the sensor assembly.

II. SENSING PRINCIPLE

The proposed sensing principle layout is depicted in Fig. 1. Two parallel LDFs are positioned at a distance d . The illuminating fiber is connected to the light source; the detection fiber is linked to the detection system. Due to the energy scattering from random imperfections in the employed light-diffusing optical fibers, there is a power-coupling mechanism enabling a power exchange between the two fibers, which can occur even when the fibers are at a very large distance in terms of optical wavelength.

The coupling between the two fibers depends on the scattering fiber properties, the distance d , and the optical properties of the medium between the fibers [36]. Using continuous source, only an average information over the entire length of the fiber is available. To get distributed measurement, in analogy with OTDR, it is necessary the use of pulsed light in the illuminating fiber. In this case, the interaction between the fibers is essentially localized to the pulse position along the fiber.

A narrow rectangular input pulse with power P_{in} arrives at the position z along the illuminating fiber with a power [19]

$$P(z) = P_{in} \exp(-\alpha z) \quad (1)$$

where $P(z)$ describes the average power in the fiber, and α is the total power attenuation coefficient along the illuminating fiber, which is a combination of attenuations due to absorption loss and scattering loss. For LDFs, the absorption losses are typically negligible compared to the scattering losses, and thus, the attenuation can be mainly attributed to the concentration of scattering particles embedded in the fiber causing side-scattering along the fiber.

The light power coupled to the detection fiber P_c , at the abscissa z , can be evaluated by using the analytical solution established in closed form in [35] for LDF coupled in the counterpropagation configuration. In this case, the coupling length is equal to spatial width H of the pulse (see Fig. 1). Taking into account that the coupling coefficient between the fiber due to the radiative transfer $\beta \ll \alpha$, P_c can be expressed as

$$P_c(z) \approx \frac{P_{in} \beta T(z)}{\alpha (1 + \coth[\alpha H])} \exp(-\alpha z) \quad (2)$$

where $T(z)$ is the transmittance of the medium between the fiber.

The power coupled $P_c(z)$ produces a signal, which arrives at the end of detection fiber with a power

$$P_{\text{out}} = P_c(z) \exp(-\alpha z) \approx \frac{P_{\text{in}} \beta T(z)}{\alpha (1 + \coth[\alpha H])} \exp(-2\alpha z). \quad (3)$$

As demonstrated in [36], in a weak-coupling regime, the coupling coefficient β between two parallel light-diffusing multimodal optical fibers of equal and finite lengths, of equal diameter D , and placed at a distance d , assumes the form

$$\beta = K \frac{(\alpha D)^2}{d} \quad (4)$$

where K is a constant that takes into account a geometric factor and the transmittance of the lateral surface of the illuminating and detection fibers. Combining (3) and (4), we can write

$$P_{\text{out}} = C P_{\text{in}} T(z) \exp(-2\alpha z) \quad (5)$$

where $C = K((\alpha D^2)/d)(1/(1 + \coth[\alpha H]))$.

According to the Lambert–Beer law, the transmittance $T(z)$ of the medium placed between the two fibers is related to the power absorption coefficient of the medium $\alpha_m(z)$ as follows:

$$T(z) = e^{-2\alpha_m(z)d}. \quad (6)$$

Equations (5) and (6) permit to directly relate the power P_{out} , measured at the end of detection fiber, with the transmittance/absorption profile along the fiber length, enabling optical absorption spectroscopy distributed measurements. If the optical pulse could not be considered narrow, the measured profile is the convolution of spatial response of fiber sensor system [instrument response function (IRF)] with the true spatial distribution of the measurand given by (5) [20], [37].

III. EXPERIMENTAL SETUP

The sensor has been assembled using two LDFs Fibrance with FC/PC connectors by Corning. This is a glass fiber designed to diffuse the light uniformly around its circumference, whereas, along the fiber length, the fiber could be assumed as a Lambertian diffuser [36]. This behavior is obtained by placing into the fiber core a ring of random distributed scattering sights with their diameters that span from 50 to 500 nm. The distance over which 90% of laser light is emitted through side scattering is called diffusion length. Two Fibrance fibers with a diffusion length of 5 m have been used. The diameters of core and cladding are 170 ± 3 and $230 \pm 10 \mu\text{m}$, respectively [38]. The fiber has a 900- μm -diameter loose tube protection jacket made of transparent polyvinyl chloride (PVC). The bending losses are also small with minimum bending radius of 5 mm. The operating wavelength range is 405–1000 nm. However, the possibility to work up to 1550 nm has also been demonstrated [35], [36], thus enabling the prospect of distributed absorption spectroscopy measurements both in the visible and in the near infrared ranges.

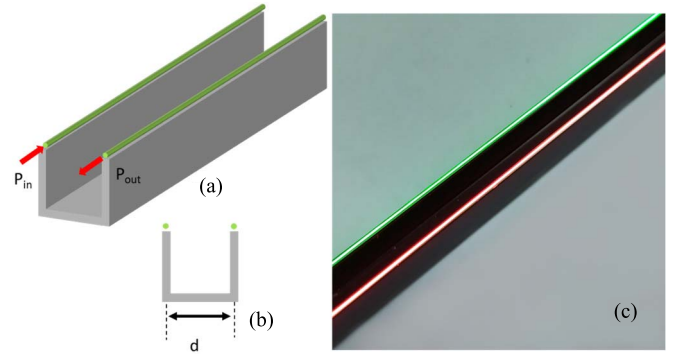


Fig. 2. (a) Sensor configuration. (b) Section view of the sensor geometry. (c) Photograph of the assembled sensor.

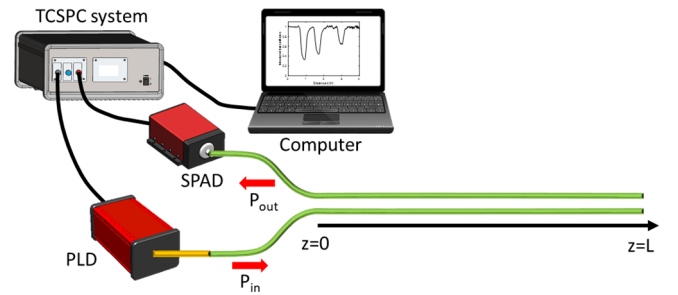


Fig. 3. Experimental setup.

The sensor configuration is illustrated in Fig. 2. The two fibers, with a total length of 5 m, are glued on the edges of a U-shaped aluminum bars (8×8 mm) (see Fig. 2), with a distance between the fibers $d = 7$ mm and a sensing length $L = 4$ m. The thickness of the bar profile is 1 mm. A picture of the assembled sensor when the illuminating and detection fibers are coupled with a green and red light source, respectively, is shown in Fig. 2(c). The bar is black painted in order to minimize unwanted light reflections. It should be noted that the proposed layout permits a simple and reliable alignment between the fibers.

The measurements have been performed by an approach similar to photon-counting OTDR. A schematic layout of the optical interrogation setup is shown in Fig. 3. A PLD at $\lambda = 850$ nm is connected to the illuminating fiber by a graded index multimode fiber with a $50 \mu\text{m}$ core diameter. The laser delivers optical pulses with a width of 83 ps [full-width half-maximum (FWHM)], at a repetition rate of 5 MHz and with an average power of 0.5 mW.

The light coupled back to the collecting fiber is delivered to a fiber-coupled single photon avalanche diode (SPAD)-based detector. Both the SPAD and the laser synchronization signals are connected to a time-correlated single photon counting (TCSPC) system (PicoHarp 300). The photon arrival histogram is collected with a time-bin width of 32 ps, corresponding to a sampling resolution of about 3.2 mm, and it is transferred to a personal computer for the signal processing. Each measurement has been repeated eight times for statistical error

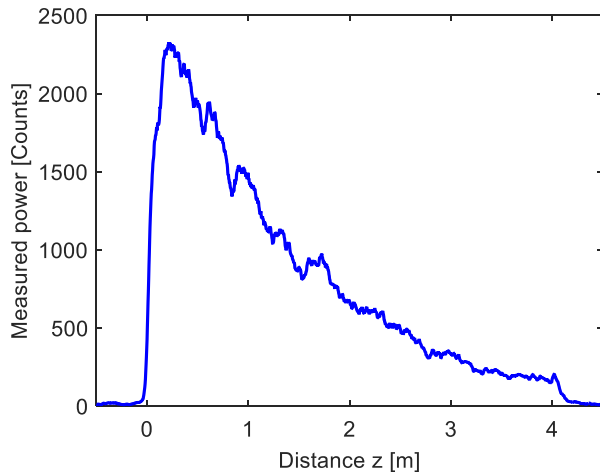


Fig. 4. Measured power when $T(z) = 1$.

analysis, and a moving average over a length of 3.2 cm was performed to remove part of the noise.

Although the Fibrance fiber exhibits a strong light scattering behavior, the possibility that very short pulse can propagate inside this fiber has been however observed [39], [40].

In Fig. 4, the case of $T(z) = 1$ (no absorbing medium between the two fibers) is addressed, and the power measured as a function of the distance is reported. An exponentially decaying of the signal according (5) is clearly visible. By fitting the data, a total attenuation coefficient $\alpha = 0.35 \text{ [m}^{-1}\text{]}$ has been evaluated, which is in good agreement with the results obtained in [36].

IV. SENSOR CHARACTERIZATION

A. Spatial Resolution

The spatial resolution represents the smallest distance of the fiber required to fully detect a localized variation step occurring to the measurand along the fiber. Typically, the spatial resolution achievable by an OTDR TCSPC-based system is assumed approximately equal to the FWHM of its IRF. The IRF summarizes its overall timing precision (spatial), and it is therefore determined by the performances of the interrogation system, such as the laser pulse duration, the photodetector, and the TCSPC electronics [37], but it is also strongly influenced by the optical properties of the system under analysis, such as the numerical aperture of the fibers [37]. In our case, the IRF has been evaluated by inserting a black screen between the fibers leaving only a small coupling region of 5 cm at $z = 1.5 \text{ m}$. Fig. 5 reports the IRF of the systems showing an FWHM of 9.3 cm.

However, in the field of distributed fiber optic sensors, the spatial resolution is typically defined as 10%–90% rise/fall transient length of the sensor response in correspondence of a sharp transition of the measurand [41]. Since the rise and fall lengths could be in generally different, the spatial resolution is evaluated as the average of the rise and fall lengths.

Fig. 6 shows the measured transmittance when a dark screen with a length of 1 m is placed between the fibers (from $z = 1.5$ to 2.5 m). The measured rise and fall length are 17.9 and 17.6 cm, respectively, with an average of 17.7 cm.

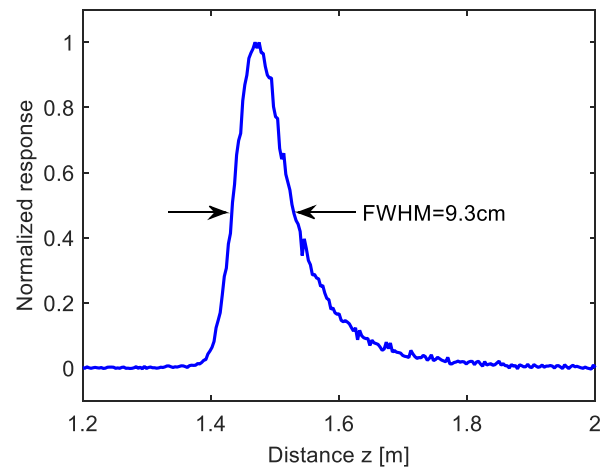


Fig. 5. Instrument response function.

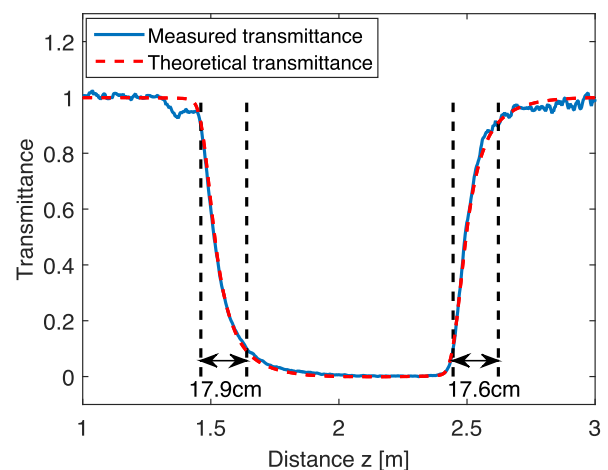


Fig. 6. Measured and theoretical evaluation of the 10%–90% rise/fall spatial resolution.

It is important to underline that the two approaches in the evaluation of spatial resolution are not in contradiction. As demonstration, the theoretical transmittance profile, evaluated as the convolution between the theoretical profile with the IRF [20], [37], is also reported in Fig. 6. As it can be observed from the figure, there is a very good agreement between the measured and the convoluted profiles.

B. Sensor Calibration

The calibration of the sensors has been performed by inserting thin-film neutral density filters (Kodak Wratten filter, thickness 0.1 mm) with a calibrated transmittance ranging from 0.082 to 1. The filters have a length of 30 cm and are placed between $z = 1.5 \text{ m}$ and $z = 1.8 \text{ m}$. The measured transmittance profiles for different filter transmission values T are reported in Fig. 7. For proper instrument calibration, the influence of the IRF on the measurements has to be taken into account. For this reason, the theoretical transmittance profiles, evaluated as the convolution between the reference profile with the IRF [20], [37], are also reported in Fig. 7.

The sensor calibration curve reporting the theoretical transmittance versus the measured transmittance is depicted in

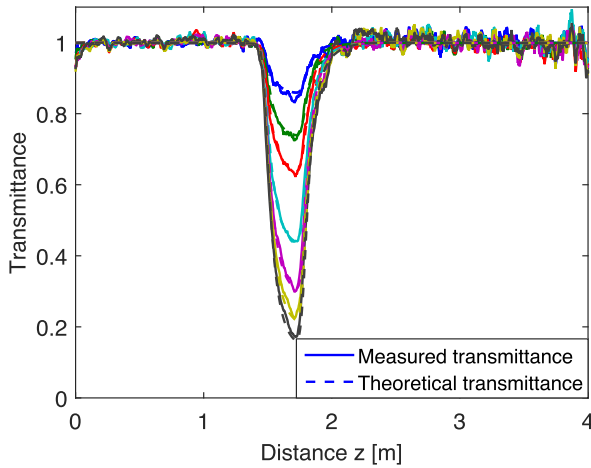


Fig. 7. Measured and theoretical transmittance profile for different transmittance values ($T = 0.85$, $T = 0.73$, $T = 0.62$, $T = 0.41$, $T = 0.27$, $T = 0.18$, and $T = 0.12$).

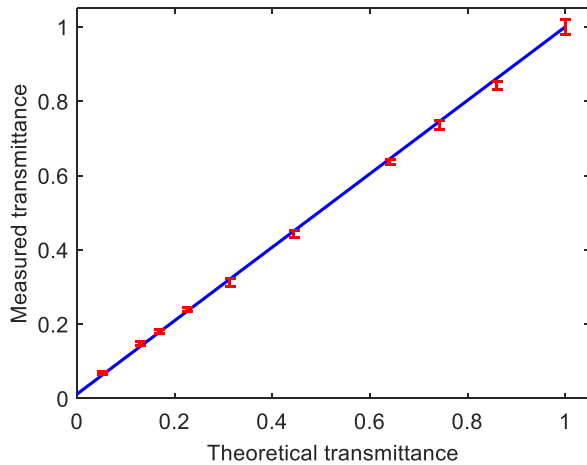


Fig. 8. Transmittance calibration curve.

Fig. 8 with the error bars that represent standard deviation evaluated over eight measurements. In Fig. 8, it is also depicted the linear fitting curve. The model fitting quality has been evaluated by the coefficient of determination R^2 , which has been found to be R -square: 0.9998.

V. DISTRIBUTED MEASUREMENTS

A. Distributed Optical Measurements

To verify the effectiveness of the proposed approach, an extensive experimental characterization has been performed by measuring different transmittance profiles along the fiber length. The profiles are synthesized by spatial combination of calibrated neutral density filters inserted between the fibers, as depicted in Fig. 9.

The first test case concerns with three different attenuation variations of decreasing value along the fiber. Each variation corresponds to 30 cm of fiber length. The measured transmittance profile along with the reference transmittance profile is reported in Fig. 10. The differences between the two profiles are essentially due to limited resolution of the system, which makes it difficult to measure profile with very sharp variation.

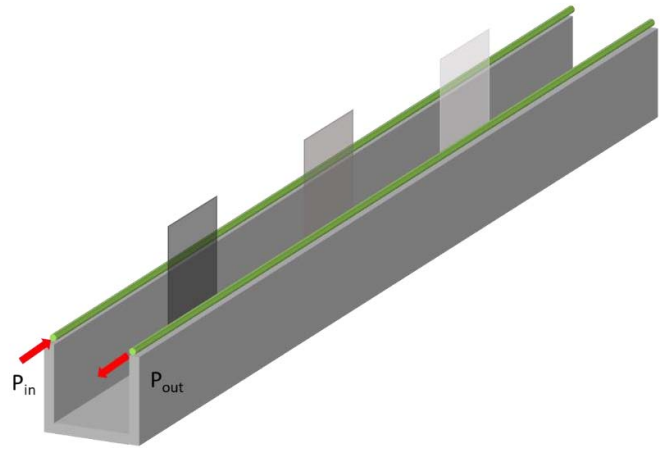


Fig. 9. Distributed transmittance measurement layout.

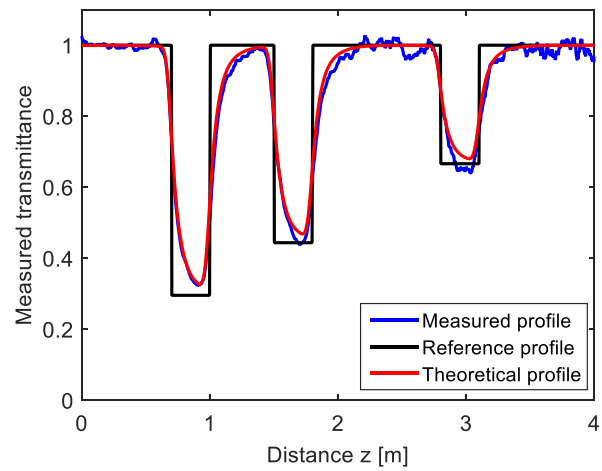


Fig. 10. Measured transmittance for a profile with three different attenuation variations of decreasing value along the fiber.

In fact, in practice, the theoretical transmittance profile is the convolution of the reference profile with the IRF [20], [37]. In order to better evaluate the accuracy of the system, in Fig. 10, the theoretical profile is also reported. As it can be observed from the figure, there is a very good agreement between the measured and the convoluted profiles. The evaluated maximum transmittance error between the two profiles is 0.05, whereas the average error is 0.016.

In the second example, the employed reference transmittance exhibits a symmetric staircase profile with two steps of 15 cm. In Fig. 11, the measured profile, the reference profile, and the theoretical profile are depicted using different colors. The evaluated maximum error is 0.050, whereas the average error is 0.015. As a more complex example, we have analyzed an asymmetric staircase profile with steps of 30 cm (see Fig. 12). In this case, the evaluated maximum error is 0.061, whereas the average error is 0.013.

Finally, we have evaluated the spatial resolution of the system by considering two transmittance perturbations with an extension of 15 cm spaced by 15 cm (see Fig. 13).

This measurement has been carried out toward the end of the sensing length, where the worst signal-to-noise-ratio is

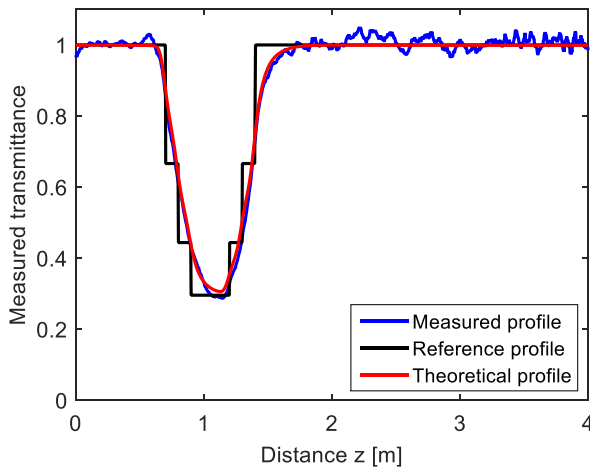


Fig. 11. Measured transmittance for a symmetric staircase profile with two steps of 15 cm.

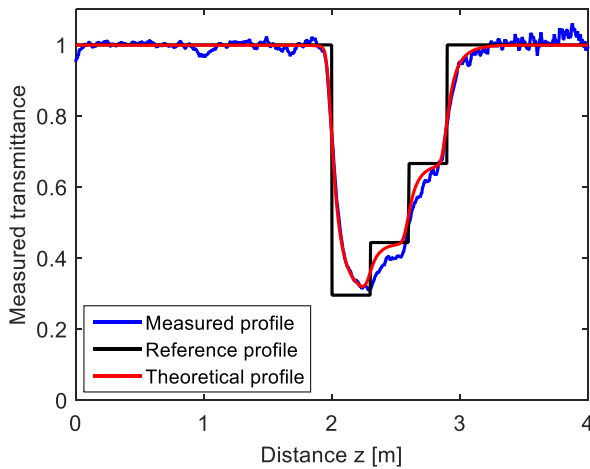


Fig. 12. Measured transmittance for asymmetric staircase profile with steps of 30 cm.

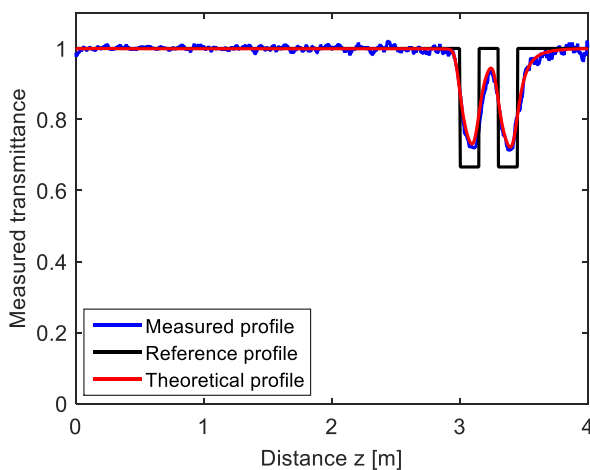


Fig. 13. Measured transmittance for two transmittance perturbations of an extension of 15 cm spaced of 15 cm profile.

achieved, so that the measured spatial resolution is effective for the entire sensing length. As it is shown in the figure, the two fiber sections are clearly resolved, confirming the estimated

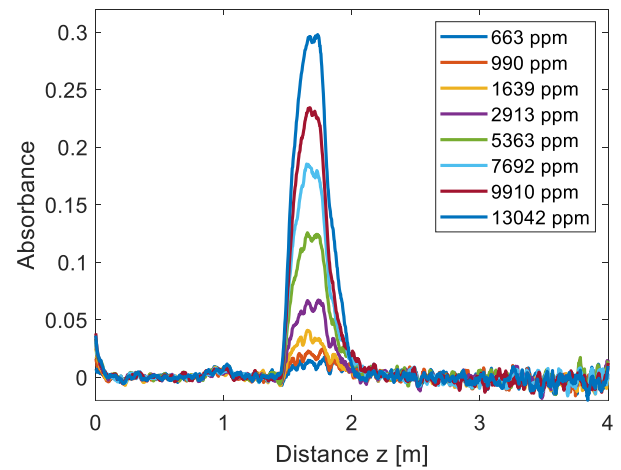


Fig. 14. Measured absorbance profiles for different copper ions concentration values.

spatial resolution. The evaluated maximum transmittance error is 0.047, whereas the average error is 0.007.

B. Distributed Chemical Measurements

In order to verify the possibility to perform distributed chemical sensing, measurements with different solutions of copper ion have been performed. Copper plays an important role in the human body. However, it could represent a dangerous pollutant as an excessive ingestion of copper may cause remarkable effects in humans, including nausea, vomiting, and diarrhea. Large amounts might damage the kidneys, inhibit urine production, and cause anemia due to the rupture of red blood cells (hemolytic anemia) and even death. The copper ions aqueous solution exhibits a broad spectral absorption band around 809 nm that could be used for sensitive detection [42].

In this case, the absorption profile is synthesized by a custom made plastic [poly(methyl methacrylate)] cuvette with a length of 30 cm and a path length of 6 mm that has been inserted between the fibers from $z = 1.5$ to 1.8 m. The plastic cuvette walls are very thin (0.5 mm) and do not affect the coupling coefficient β between the optical fibers.

According to the Lambert–Beer law, the absorbance A is related to the concentration C of the absorbing substance as follows:

$$A = \varepsilon(\lambda)Cd \quad (7)$$

where $\varepsilon(\lambda)$ is the molar absorption coefficient of the absorbing substance at the working wavelength and d is the thickness of the absorbing layer.

Copper ions solutions were prepared by dissolving copper(II) nitrate trihydrate (Sigma-Aldrich) in bidistilled water. The experimental measurements have been performed by filling the cuvette with solutions concentration spanning from 663 to 13042 ppm. For each concentration, eight repeated measurements have been performed. The measured absorbance profiles are shown in Fig. 14. From the absorbance peak values calculated at each concentration, a calibration curve has been constructed (see Fig. 15). The error bars reported in the figure represent the measurement standard deviation evaluated over

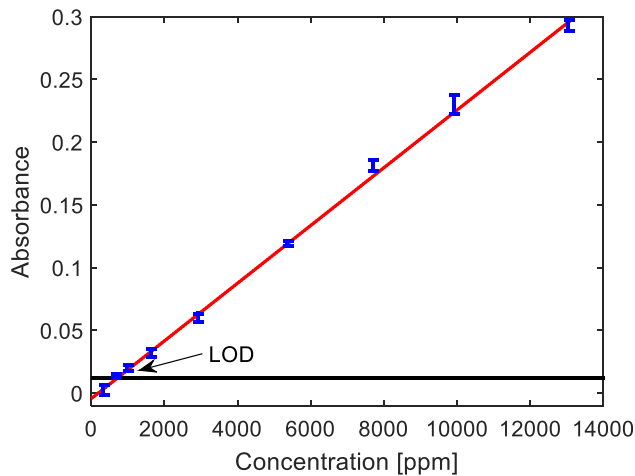


Fig. 15. Measured absorbance versus copper ions concentration value.

eight measurements. A linear regression of the data has been performed, and an R -square = 0.9986 has been obtained. From the slope of the linear fit, we have calculated an absorbance sensitivity of 2.3×10^{-5} [1/ppm]. The limit of detection (LOD) has been determined as the concentration of analyte, which gives a signal 3σ above the mean blank signal, i.e., the signal of pure water (where σ is the standard deviation of the blank signal). The LOD determined for copper ions in water is 710 ppm.

VI. CONCLUSION

A distributed fiber optic sensing approach for optical absorption spectroscopy and chemical sensing has been proposed and validated for the first time. The sensor is based on two light diffusing optical fibers that are radiatively coupled by scattering from random imperfections in the fibers. The proposed configuration requires a very simple approach for sensor fabrication and does not require any manipulation of the optical fiber, such as cladding removal, etching or bending. By an OTDR TCSPC-based interrogation system, the sensor is able to perform distributed optical measurements of the transmission/absorption properties of the medium between the fibers with a spatial resolution of about 17 cm along a 4-m length fiber. The application to distributed chemical sensing has also been demonstrated. The sensor permits to monitor the concentration of copper ions in water with an LOD of 710 ppm. Future studies will be devoted to extend the proposed approach to near infrared range up to 2500 nm and to understand how the proposed sensor could be applied to the detection of other pollutants (e.g., ammonia, bacteria, etc.) [43], [44], [45], [46].

REFERENCES

- [1] A. Shadab, S. K. Raghuvanshi, and S. Kumar, "Advances in micro-fabricated fiber Bragg grating for detection of physical, chemical, and biological parameters—A review," *IEEE Sensors J.*, vol. 22, no. 16, pp. 15650–15660, Aug. 2022.
- [2] V. S. Chaudhary, D. Kumar, G. P. Mishra, S. Sharma, and S. Kumar, "Plasmonic biosensor with gold and titanium dioxide immobilized on photonic crystal fiber for blood composition detection," *IEEE Sensors J.*, vol. 22, no. 9, pp. 8474–8481, May 2022.
- [3] V. S. Chaudhary, D. Kumar, and S. Kumar, "Gold-immobilized photonic crystal fiber-based SPR biosensor for detection of malaria disease in human body," *IEEE Sensors J.*, vol. 21, no. 16, pp. 17800–17807, Aug. 2021.
- [4] V. S. Chaudhary, D. Kumar, and S. Kumar, "SPR-assisted photonic crystal fiber-based dual-wavelength single polarizing filter with improved performance," *IEEE Trans. Plasma Sci.*, vol. 49, no. 12, pp. 3803–3810, Dec. 2021.
- [5] R. Srivastava, Y. K. Prajapati, S. Pal, and S. Kumar, "Micro-channel plasmon sensor based on a D-shaped photonic crystal fiber for malaria diagnosis with improved performance," *IEEE Sensors J.*, vol. 22, no. 15, pp. 14834–14841, Aug. 2022.
- [6] M. S. Soares et al., "Immunosensing based on optical fiber technology: Recent advances," *Biosensors* vol. 11, p. 305, Aug. 2021.
- [7] Y. Wang et al., "Cardiac troponin I detection using gold/cerium-oxide nanoparticles assisted hetero-core fiber structure," *IEEE Trans. Nanobiosci.*, early access, Jul. 19, 2022, doi: 10.1109/TNB.2022.3192491.
- [8] M. Li, R. Singh, M. S. Soares, C. Marques, B. Zhang, and S. Kumar, "Convex fiber-tapered seven core fiber-convex fiber (CTC) structure-based biosensor for creatinine detection in aquaculture," *Opt. Exp.*, vol. 30, no. 8, pp. 13898–13914, Apr. 2022.
- [9] T. Horiguchi, K. Shimizu, T. Kurashima, M. Tateda, and Y. Koyamada, "Development of a distributed sensing technique using Brillouin scattering," *J. Lightw. Technol.*, vol. 13, no. 7, pp. 1296–1302, Jul. 1995.
- [10] P. Lu et al., "Distributed optical fiber sensing: Review and perspective," *Appl. Phys. Rev.*, vol. 6, Dec. 2019, Art. no. 041302.
- [11] M. E. Froggatt and J. Moore, "High-spatial-resolution distributed strain measurement in optical fiber with Rayleigh scatter," *Appl. Opt.*, vol. 37, no. 10, pp. 1735–1740, 1998.
- [12] A. Minardo, R. Bernini, and L. Zeni, "Experimental and numerical study on stimulated Brillouin scattering in a graded-index multimode fiber," *Opt. Exp.*, vol. 22, pp. 17480–17489, Jul. 2014.
- [13] Y. Mizuno, A. Theodosiou, K. Kalli, S. Liehr, H. Lee, and K. Nakamura, "Distributed polymer optical fiber sensors: A review and outlook," *Photon. Res.*, vol. 9, no. 9, pp. 1719–1733, 2021.
- [14] A. Minardo, R. Bernini, and L. Zeni, "Distributed temperature sensing in polymer optical fiber by BOFDA," *IEEE Photon. Technol. Lett.*, vol. 26, no. 4, pp. 387–390, Dec. 12, 2014.
- [15] T. Chen et al., "Distributed hydrogen sensing using in-fiber Rayleigh scattering," *Appl. Phys. Lett.*, vol. 100, May 2012, Art. no. 191105.
- [16] M. K. Barnoski and S. M. Jensen, "Fiber waveguides: A novel technique for investigating attenuation characteristics," *Appl. Opt.*, vol. 15, no. 9, p. 2112, 1976.
- [17] J. P. Dakin, D. J. Pratt, G. W. Bibby, and J. N. Ross, "Distributed optical fibre Raman temperature sensor using a semiconductor light source and detector," *Electron. Lett.*, vol. 21, no. 13, pp. 569–570, Jun. 1985.
- [18] T. Horiguchi and M. Tateda, "BOTDA-nondestructive measurement of single-mode optical fiber attenuation characteristics using Brillouin interaction: Theory," *J. Lightw. Technol.*, vol. 7, no. 8, pp. 1170–1176, Aug. 1989.
- [19] D. Marcuse, *Principles of Optical Fiber Measurements*. New York, NY, USA: Academic, 1981.
- [20] A. H. Hartog, *An Introduction to Distributed Optical Fibre Sensors*. Boca Raton, FL, USA: CRC Press, 2017.
- [21] J. C. Juarez, E. W. Maier, K. N. Choi, and H. F. Taylor, "Distributed fiber-optic intrusion sensor system," *J. Lightw. Technol.*, vol. 23, no. 6, pp. 2081–2087, Jun. 13, 2005.
- [22] X. Lu, P. J. Thomas, and J. O. Hellevang, "A review of methods for fibre-optic distributed chemical sensing," *Sensors*, vol. 19, no. 13, p. 2876, Jun. 2019.
- [23] R. A. Lieberman, "Distributed and multiplexed chemical fiber optic sensors," *Proc. SPIE*, vol. 1586, pp. 80–91, Jan. 1992.
- [24] A. MacLean, C. Moran, W. Johnstone, B. Culshaw, D. Marsh, and G. Andrews, "Distributed fiber optic sensor for liquid hydrocarbon detection," *Proc. SPIE*, vol. 4328, pp. 47–53, Aug. 2001.
- [25] R. A. Lieberman et al., "Intrinsic fiber optic sensor for distributed water detection," *Proc. SPIE*, vol. 2068, pp. 192–201, Mar. 1994.
- [26] R. A. Lieberman, L. L. Blyler, and L. G. Cohen, "A distributed fiber optic sensor based on cladding fluorescence," *J. Lightw. Technol.*, vol. 8, no. 2, pp. 212–220, Feb. 1990.
- [27] F. Lu, R. Wright, P. Lu, P. C. Cvetič, and P. R. Ohodnicki, "Distributed fiber optic pH sensors using sol-gel silica based sensitive materials," *Sens. Actuators B, Chem.*, vol. 340, Aug. 2021, Art. no. 129853.

- [28] C. A. Browne, D. H. Tarrant, M. S. Olteanu, J. W. Mullens, and E. L. Chronister, "Intrinsic sol-gel clad fiber-optic sensors with time-resolved detection," *Anal. Chem.*, vol. 68, no. 14, pp. 2289–2295, Jan. 1996.
- [29] R. A. Potyrailo and G. M. Hieftje, "Optical time-of-flight chemical detection: Absorption-modulated fluorescence for spatially resolved analyte mapping in a bidirectional distributed fiber-optic sensor," *Anal. Chem.*, vol. 70, no. 16, pp. 3407–3412, Aug. 1998.
- [30] W. Jin, H. L. Ho, Y. C. Cao, J. Ju, and L. F. Qi, "Gas detection with micro- and nano-engineered optical fibers," *Opt. Fiber Technol.*, vol. 19, no. 6, pp. 741–759, Dec. 2013.
- [31] O. Thomas and C. Burgess, *UV-Visible Spectrophotometry of Water and Wastewater*, 2nd ed. Amsterdam, The Netherlands: Elsevier, 1998.
- [32] C. Pasquini, "Near infrared spectroscopy: A mature analytical technique with new perspectives—A review," *Analytica Chim. Acta*, vol. 1026, pp. 8–36, Oct. 2018.
- [33] S. Logunov, E. Fewkes, F. Shustack, and F. Wagner, "Light diffusing optical fiber for illumination," in *Proc. Solid-State Organic Lighting*, Washington, DC, USA, 2013, pp. 1–3.
- [34] N. Cennamo et al., "Biosensors exploiting unconventional platforms: The case of plasmonic light-diffusing fibers," *Sens. Actuators B, Chem.* vol. 337, Jun. 2021, Art. no. 129771.
- [35] P. Imperatore, G. Persichetti, G. Testa, and R. Bernini, "Continuous liquid level sensor based on coupled light diffusing fibers," *IEEE J. Sel. Topics Quantum Electron.*, vol. 26, no. 4, pp. 1–8, Jul. 2020.
- [36] P. Imperatore, G. Testa, G. Persichetti, and R. Bernini, "Power coupling between light diffusing fibers: Modelling and validation," *J. Lightw. Technol.*, vol. 40, no. 3, pp. 813–821, Feb. 1, 2022.
- [37] W. Becker, *Advanced Time-Correlated Single Photon Counting Techniques*. Cham, Switzerland: Springer, 2005.
- [38] *Corning Fibrance Light Diffusing Fiber, Specification Datasheet*. Accessed: 2022. [Online]. Available: <https://www.corning.com/media/worldwide/Innovation/documents/FibranceSpecificationSheet082116.pdf>
- [39] R. Warburton et al., "Observation of laser pulse propagation in optical fibers with a SPAD camera," *Sci. Rep.*, vol. 7, no. 1, p. 43302, 2017.
- [40] X. Feng and L. Gao, "Ultrafast light field tomography for snapshot transient and non-line-of-sight imaging," *Nature Commun.*, vol. 12, no. 1, p. 2179, Apr. 2021.
- [41] A. Minardo, R. Bernini, and L. Zeni, "Numerical analysis of single pulse and differential pulse-width pair BOTDA systems in the high spatial resolution regime," *Opt. Exp.*, vol. 19, no. 20, p. 19233, 2011.
- [42] S.-C. Hung, C.-C. Lu, and Y.-T. Wu, "An investigation on design and characterization of a highly selective LED optical sensor for copper ions in aqueous solutions," *Sensors*, vol. 21, no. 4, p. 1099, Feb. 2021.
- [43] C. Leitão et al., "Cortisol AuPd plasmonic unclad POF biosensor," *Biotechnol. Rep.*, vol. 29, Mar. 2021, Art. no. e00587.
- [44] A. G. Leal-Junior, A. Frizzera, and C. Marques, "Low-cost fiberoptic probe for ammonia early detection in fish farms," *Remote Sens.*, vol. 12, no. 9, p. 1439, May 2020.
- [45] Z. Wang, R. Singh, C. Marques, R. Jha, B. Zhang, and S. Kumar, "Taper-in-taper fiber structure-based LSPR sensor for alanine aminotransferase detection," *Opt. Exp.*, vol. 29, no. 26, pp. 43793–43810, Dec. 2021.
- [46] S. Kumar et al., "MoS₂ functionalized multicore fiber probes for selective detection of Shigella bacteria based on localized plasmon," *J. Lightw. Technol.*, vol. 39, no. 12, pp. 4069–4081, Jun. 15, 2021.

Gianluca Persichetti received the Laurea degree and the Ph.D. degree in novel technologies for materials sensors and imaging from the University of Naples Federico II, Naples, Italy, in 2003 and 2010, respectively.

He is currently a Senior Researcher with the Institute for Electromagnetic Sensing of the Environment (IREA), National Research Council of Italy (CNR), Naples. He is also a Physicist. A primary focus of his work is on the development of optofluidic sensors based on Raman and fluorescence spectroscopy. Another part of his activity is aimed at the development of sensors based on optical waveguides, ranging from optical fiber sensors to polymer waveguides manufactured by photolithographic processes.

Genni Testa received the Laurea (summa cum laude) degree in solid states physics from the University of Naples Federico II, Naples, Italy, in 2005, and the Ph.D. degree in electrical engineering from the Second University of Naples, Aversa, Italy, in 2008.

She is currently a Researcher with the Institute for the Electromagnetic Sensing of the Environment (IREA), Italian National Research Council (CNR), Naples. She is the author or a coauthor of more than 30 international journal articles. Her research activities deal with the design, fabrication, and characterization of microfluidic and optofluidic devices for biosensing and environmental applications.

Dr. Testa acts as a reviewer of several international journals.

Pasquale Imperatore (Member, IEEE) received the Laurea (summa cum laude) degree in electronic engineering and the Ph.D. degree in electronic and telecommunication engineering from the University of Naples Federico II, Naples, Italy, in 2001 and 2010, respectively.

He is the Research Scientist of the Institute for Electromagnetic Sensing of the Environment (IREA), National Research Council of Italy (CNR), Naples. He has co-edited two books in the field of remote sensing and geospatial technology. His research interests include electromagnetics and microwave remote sensing, with a particular emphasis on theoretical models, scattering in random layered media, synthetic aperture radar (SAR) data modeling and processing, SAR interferometry, parallel algorithms, and high-performance computing (HPC).

Dr. Imperatore acts as a reviewer of several peer-reviewed journals.

Romeo Bernini (Member, IEEE) received the Laurea (summa cum laude) degree from the University of Naples Federico II, Naples, Italy, in 1995, and the Ph.D. degree in electronic engineering from the Second University of Naples, Aversa, Italy, in 1999.

He was a Research Fellow with the Second University of Naples in 2000. He is currently the Research Director of the Institute for the Electromagnetic Sensing of the Environment (IREA), Italian National Research Council (CNR), Naples. He has authored or coauthored more than 100 articles published in various international journals. He holds one international and two national patents on fiber optic sensors. He is/was responsible of many international and national projects in the field of optical sensors for physical and chemical applications. His research fields are optoelectronic devices and sensors, microfluidic and optofluidic devices, and fiber optic sensors.

Dr. Bernini is a reviewer of several technical journals.